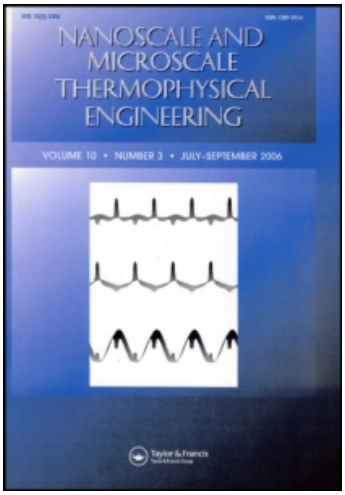

Nanoscale and Microscale Thermophysical Engineering
Publication details, including instructions for authors and subscription information:
http://www.informaworld.com/smpp/title~content=t713774103

Effects of Nano- to Micropore Diameter on Water Vapor Transport Diffusivities Within Porous Polycarbonate Barriers

Matthew J. Traum[a]; Edwin L. Thomas[b]; William A. Peters[c]
[a] Department of Mechanical Engineering, Milwaukee School of Engineering, Milwaukee, Wisconsin [b] Institute for Soldier Nanotechnologies and Department of Materials Science and Engineering, Massachusetts Institute of Technology, Cambridge, Massachusetts, USA [c] Institute for Soldier Nanotechnologies, Massachusetts Institute of Technology, Cambridge, Massachusetts, USA

Online publication date: 29 April 2011

To cite this Article Traum, Matthew J. , Thomas, Edwin L. and Peters, William A.(2011) 'Effects of Nano- to Micropore Diameter on Water Vapor Transport Diffusivities Within Porous Polycarbonate Barriers', Nanoscale and Microscale Thermophysical Engineering, 15: 2, 123 — 131
To link to this Article: DOI: 10.1080/15567265.2011.575917
URL: http://dx.doi.org/10.1080/15567265.2011.575917

Nanoscale and Microscale Thermophysical Engineering, 15: 123–131, 2011

ISSN: 1556-7265 print / 1556-7273 online
DOI: 10.1080/15567265.2011.575917

EFFECTS OF NANO- TO MICROPORE DIAMETER ON WATER VAPOR TRANSPORT DIFFUSIVITIES WITHIN POROUS POLYCARBONATE BARRIERS

Matthew J. Traum[1], Edwin L. Thomas[2], and William A. Peters[3]
[1]*Department of Mechanical Engineering, Milwaukee School of Engineering, Milwaukee, Wisconsin*
[2]*Institute for Soldier Nanotechnologies and Department of Materials Science and Engineering, Massachusetts Institute of Technology, Cambridge, Massachusetts*
[3]*Institute for Soldier Nanotechnologies, Massachusetts Institute of Technology, Cambridge, Massachusetts*

Effective pore diffusivities for dilute water vapor in air were measured at atmospheric pressure and 30°C by continuously weighing an evaporator capped with a porous polycarbonate barrier and correcting steady-state water vapor fluxes for apparatus mass transfer resistances. The Knudsen number was increased from 0.018 to 2.4 at constant pressure by decreasing pore diameter from 5,400 to 39 nm, thus increasing the influence of vapor molecule collisions with pore walls on mass transport. Correspondingly, diffusivities decreased in qualitative accord with a model equating total pore diffusion resistance to the sum of the continuum diffusion (*Kn $<$ *0.01) and Knudsen diffusion (*Kn $>$ *10) resistances. Correction for irregular pore geometry with a best-fit tortuosity (∼4) significantly improved agreement between measured and predicted diffusivities.

KEY WORDS: nanopore, Knudsen diffusion, continuum diffusion, tortuosity, track-etched porous barriers, water vapor

INTRODUCTION

Gas and condensable vapor transport in nanoporous solids affects energy conversion technologies [1], air purification and cooling [2], gas separations [3–6], fluid–solids reaction engineering [7–9], adsorption processes [8], water desalination [10], and evaporative cooling of surfaces covered by ballistic, blast or chem/bioprotection gear [11–13]. There is need for fundamental understanding of how pore shape, surface properties, and diameter, d ($=2r$) affect net transport through the solids for pressures, mass transfer rates, heat

Received 25 November 2010; accepted 24 March 2011.
This research was supported by the U.S. Army, through the Institute for Soldier Nanotechnologies, under Contract DAAD-19-02-D-0002 with the U.S. Army Research Office. The content does not necessarily reflect the position of the government, and no official endorsement should be inferred. We thank Dr. Steven Kooi for preparation and imaging of barrier samples, Dr. Catherine Byrne for assistance in developing the experimental apparatus, and Professor Peter Griffith for helpful comments.
Address correspondence to Matthew J. Traum, Department of Mechanical Engineering, Milwaukee School of Engineering, 1025 N. Broadway, Milwaukee, WI 53202-3109. E-mail: mtraum@alum.mit.edu

loads, and vapor compositions of practical significance. However, nanoscale pore diameters complicate interpretation. When the pore Knudsen number (*Kn*), that is, the ratio of the gas mean free path λ (where λ scales inversely with pressure) to d, exceeds 0.01, gas rarefaction phenomena affect transport [14–17]. Molecular (bulk) diffusion, caused by collisions between gas molecules, is independent of d, but the Knudsen diffusive flux, caused by gas collisions with pore walls, scales as r^3 and at sufficiently small r can overtake the Hagen-Poiseuille (i.e., pressure driven) flux, which scales as r^4, even up to pressures of 0.1 MPa [8]. Other effects of tiny length scales are surface roughness when the gas de Broglie wavelength is less than the size of surface irregularities [17] and nonnegligible statistical fluctuations in macroscopic state quantities when d is below 20δ, where δ is the mean spacing of the gas molecules $= n^{-1/3}$ and n is the molecular number density [15]. Moreover, interfacial curvature [1, 18, 19] can change chemical potential gradients that drive vapor transport through pores, because vapor pressure, surface tension, and heat of vaporization, respectively, scale as: $\exp(\pm 1/r)$ [1, 8, 9, 18–20]; $\pm 1/r$ and $1/r^2$ [1, 18, 19, 21, 22]; and $\pm 1/r$ and $-1/r^4$ [18] where surface convexity determines the signs. Even without wall curvature, pores of width w comparable to molecular dimensions can modify diffusion driving forces [8, 9, 23, 24]. For example, molecular simulations of water confined at 300 K in 0.4- to 1.6-nm-wide *flat* channels [24] showed that capillary evaporation depends on total pressure and w for hydrophobic walls, whereas hydrophilic walls prevent ice formation and cavitation observed in bulk water. This article focuses on impacts of the r dependence of the Knudsen diffusion coefficient on water vapor transport in nano- and micropores.

BACKGROUND AND MOTIVATION

Past experiments to study rarefaction effects on gas transport in channels have increased *Kn* by reducing total pressure (to ~0.5 Pa) in fixed diameter silica or metal capillary tubes [16, 25–27] or have imposed pressure gradients across silicon or polymer barriers of a single pore diameter [29, 30]. Thin, organic–polymer barriers with a range of nano-diameter through-pores (10–12,000 nm with low size dispersion) can now be obtained and imaged to nanometer resolution. This allows rarefaction effects on pore diffusion in soft materials to be systematically studied by decreasing d at fixed pressure. Thus, high *Kn* can be investigated at elevated pressures (e.g., $\geq$0.1 MPa), which is of practical interest in micro- and nanodevices [15] and which marginalize statistical fluctuations in the gas because n is large. Here we report on the use of this approach to quantify how pore diffusivity of water vapor is affected by a roughly 140-fold variation in d from 39 nm (about 100 molecular diameters) to 5,400 nm. The results are applicable to evaporative cooling of surfaces protected by nano-engineered porous overlays [12, 13] and to gas and vapor transport in porous solids used in adsorption and heterogeneous catalysis [8]. Using a mathematical model to disaggregate the effects of apparatus mass transfer resistances from pore transport, we deduced effective pore diffusion coefficients $\left(D^P_{H_2O-Air,eff} = D^P_{H_2O-Air}/\tau\right)$ for dilute water vapor, 3.5–7.1 mol% in air at 0.1 MPa total pressure in hydrophilic polycarbonate (PC) barriers (1.4–32.0% porosity, 6.3–21.3 μm thick), at 307 $\pm$ 9 K for $2.4 \geq Kn \geq 0.018$. The superscript P denotes a property within the pores, and τ is the tortuosity, a parameter to account for variability in pore orientation, cross-sectional area, and shape [7, 8]. Figure 1 shows a scanning electron micrograph (SEM) image of an $18.4 \pm 0.2-\mu$m-thick PC barrier with $d = 95 \pm 14$ nm that was cross-section polished in an argon ion polisher.

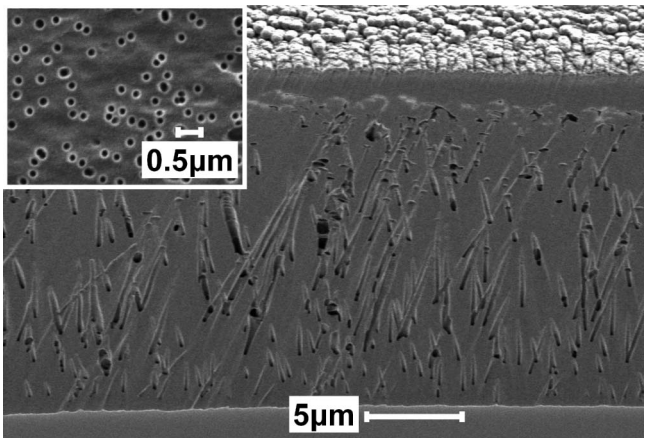

Figure 1 SEM images of an 18.4 ± 0.2-µm-thick polycarbonate barrier with track-etched pores of 95 ± 14 nm diameter. The main image shows internal pore features revealed using argon-ion cross-section polishing. The exposed edge face was imaged at 45° to the incoming electron beam and shows that the pores run straight through between the two faces of the barrier but also that some pore axes are off-normal to the barrier face (by as much as 80°; see text) and that some pore paths intersect. These features increase the diffusion path length and the mass transfer resistance of the barrier. The inset is a top-down image of the same barrier.

EXPERIMENT

Our experiments [12] applied a known, constant heat flux density to the underside of a 42-mm-diameter by 2.1-mm-deep pool of deionized liquid water in a shallow cylindrical evaporation chamber (Figure 2) sealed at its top with a barrier. The cumulative weight loss $m_{tot}(t)$ versus time due to water evaporation and transport to ambient through the barrier's pores was measured by continuously monitoring the weight of the evaporator. Assuming that mass transfer resistances are series additive, the steady-state flux of water vapor through the pores, $dm_{tot}(t)/dt$, is

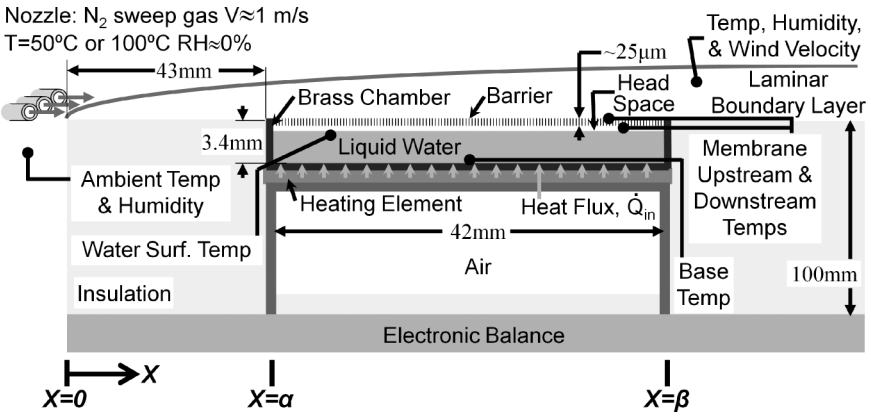

Figure 2 Schematic (not to scale) of evaporator apparatus for determining diffusion coefficients for water vapor in air in nanoscale pores. The coordinate system used for the integration of Eq. (5) is given at the bottom of the schematic.

$$\frac{dm_{tot}(t)}{dt} = \frac{A(\rho_o - \rho_{amb})}{R_{bar} + R_{US} + R_{DS}} \quad (1)$$

Here, A is the *total* area of the barrier face; ρ_o and ρ_{amb} are the mass density of water vapor at the liquid water–air interface and in the ambient gas outside the evaporator; and R_{bar}, R_{US}, and R_{DS} are, respectively, the steady-state resistances to water vapor mass transport within the barrier, in the region between the liquid water surface and the barrier entrance (upstream [US] of barrier with respect to the diffusion direction), and across a concentration boundary layer (BL) between the barrier exit and the ambient (downstream [DS] of the barrier with respect to the diffusion direction). This BL was formed by sweeping dry, preheated N_2 gas across the evaporator exit to keep the barrier pore temperature above the water dew point and to minimize ρ_{amb}, which was taken as zero. The quantity ρ_o was calculated from the vapor pressure of pure liquid water at the temperature of the liquid water at its air interface (Figure 2).

After R_{US} and R_{DS} were calculated, R_{bar} was determined from Eq. (1), taking $dm_{tot}(t)/dt$ as the slope of the $m_{tot}(t)$ versus t curve and estimating temperature inside the pores as the arithmetic mean of the measured entrance and exit face temperatures. The effective transport diffusivity $D^P_{H_2O-Air}/\tau$ was then calculated from Eq. (2):

$$\frac{D^P_{H_2O-Air}}{\tau} = \frac{L}{\varepsilon_v \cdot R_{bar}} \quad (2)$$

Table 1 presents measured values of the porosity ε_v, thickness L, and pore diameter of each nano- and microporous PC barrier along with measured effective transport diffusivities for dilute water vapor in 0.1 MPa air in the pores. An average τ was estimated for the present barriers as described below.

A gap of depth L_{US} between the liquid water–air interface and the barrier entrance prevents liquid water from wicking into the barrier pores, but it also creates a resistance to water vapor mass transfer, R_{US}.

Table 1 Physical characteristics of nano- and microporous polycarbonate barriers and measured effective transport diffusivities ($D^P_{H_2O-Air}/\tau$) for dilute water vapor in 0.1 MPa air in the barrier pores as determined from Eq. (2)

Pore diameter (nm)	Thickness (μm)	Porosity (%)	Diffusivity (m^2/s)[a]
5,400 ± 500	16.6 ± 0.2	15.4 ± 1.7	$6.0 \pm 3.7 \times 10^{-6}$
890 ± 30	18.8 ± 0.2	32.0 ± 1.3	$5.4 \pm 3.7 \times 10^{-6}$
700 ± 50	21.3 ± 0.2	22.3 ± 1.3	$5.9 \pm 2.7 \times 10^{-6}$
410 ± 20	8.8 ± 0.2	17.3 ± 2.5	$3.1 \pm 1.2 \times 10^{-6}$
410 ± 20	8.8 ± 0.2	17.3 ± 2.5	$3.4 \pm 1.6 \times 10^{-6}$
150 ± 20	19.4 ± 0.2	27.5 ± 1.3	$3.5 \pm 1.4 \times 10^{-6}$
95 ± 14	18.4 ± 0.2	13.6 ± 1.6	$6.5 \pm 3.0 \times 10^{-6}$
95 ± 14	18.4 ± 0.3	13.7 ± 1.6	$2.2 \pm 0.4 \times 10^{-6}$
60 ± 9	19.7 ± 0.2	5.9 ± 1.7	$5.1 \pm 2.0 \times 10^{-6}$
60 ± 9	21.3 ± 0.3	5.8 ± 1.8	$5.1 \pm 1.6 \times 10^{-6}$
39 ± 13	6.3 ± 0.3	1.4 ± 0.6	$1.8 \pm 0.7 \times 10^{-6}$

[a]Average of three or more separate determinations.

$$R_{US} = \frac{L_{US}}{D^{US}_{H_2O-Air}} \tag{3}$$

$D^{US}_{H_2O-Air}$ is the molecular diffusivity of water vapor in air [31] at the measured conditions upstream of the barrier (and downstream $D^{DS}_{H_2O-Air}$; Eq. (4)). During a typical 20-min steady-state run, water evaporation increased L_{US} and thus R_{US} by $\leq$20%. This caused the total mass transfer resistance ($R_{bar} + R_{US} + R_{DS}$) at the end of a run to increase by no more than 11.5%. Generally the increases were considerably less because in runs with smaller ID pores R_{US} represent a smaller fraction of ($R_{bar} + R_{US} + R_{DS}$). Moreover $dm_{tot}(t)/dt$ in Eq. (1) was determined from $m_{tot}(t)$ vs. t data during earlier stages of the steady-state evaporation period and did not deviate significantly from linearity [12]. Thus, L_{US} was treated as constant in Eq. (3).

Tracer measurements and Reynolds number calculations show that the flow of N_2 sweep gas (1.0 $\pm$ 0.15 m/s, nozzle exit temperatures of 50°C or 100°C) created a laminar BL on the DS faces of the barrier and its surrounding flat plate (Figure 2). R_{DS} was calculated from the properties of this BL:

$$R_{DS} = \frac{\beta - \alpha}{\overline{Sh_L} \cdot D^{DS}_{H_2O-Air}} \tag{4}$$

α and β, respectively, are the distances from the beginning of the BL (the leading edge of a flat plate) to the two sides of the barrier; that is, $(\beta - \alpha) = D$, the barrier diameter (Figure 2). $\overline{Sh_L}$ is the average Sherwood number, Sh, for mass transfer occurring in laminar flow over a horizontal flat plate, estimated by numerically integrating a correlation [31] for the corresponding position (x)-dependent Sh over the barrier diameter, where x is the spatial coordinate parallel to the sweep gas flow, and the momentum BL begins on the flat plate surrounding the barrier at $x = 0$ (Figure 2).

$$\overline{Sh_L} = \frac{1}{\beta - \alpha} \int_{\alpha^+}^{\beta} \frac{0.331 \mathrm{Re}_x^{\frac{1}{2}} Sc^{\frac{1}{2}}}{\left[1 - \left(\frac{\alpha}{x}\right)^{\frac{3}{4}}\right]^{\frac{1}{3}}} dx \quad x > \alpha \tag{5}$$

Here, Re_x is the Reynolds number for laminar flow over a flat plate in the x-direction and Sc is the Schmidt number for dilute water vapor in nitrogen. To calculate a practical average mass transport resistance for the mass boundary layer while avoiding a singularity in Eq. (5) at $x = \alpha$, the lower limit of integration was taken at α^+ where $(\alpha^+ - \alpha) = 1$ mm or 2.4% of the barrier diameter. Typical values of R_{US}, R_{DS}, and R_{bar} were 34.9–50.7, 45.1–62.5, and 10.9–248.6 s/m, respectively. R_{bar} increased as d decreased.

THEORETICAL MODELING

For $0.01 \leq Kn \leq 10$, sometimes referred to as the *transition region*, it is reasonable to assume that gases transmit momentum along a pore by the combined effects of collisions between gaseous molecules (the mechanism of gas phase molecular diffusion) and by molecule–wall collisions (the Knudsen diffusion mechanism) [8, 17]. The total diffusion resistance of a pore $1/D^{P}_{H_2O-Air}$ can then be equated to the sum of the molecular

diffusion resistance, $1/D_{H_2O-Air}$, and the Knudsen diffusion resistance, $1/D_{Kn}$, of the pore (D_i is the corresponding diffusion coefficient) [7, 8, 31]; that is,

$$\frac{1}{D^P_{H_2O-Air}} = \left(\frac{1}{D_{H_2O-Air}} + \frac{1}{D_{Kn}}\right); 0.01 \leq Kn \leq 10 \tag{6}$$

D_{H_2O-Air} is independent of pore diameter but, to first order, D_{Kn} is directly proportional to d [16], which allows prediction of pore size effects on $D^P_{H_2O-Air}$. Equation (6) is an approximation, valid for pores of regular geometry (see below) and when net transport occurs by equimolar counterdiffusion or, as is true here, when convection caused by diffusion (the Stefan flow) is small [8] (calculated at <4% of the diffusive flux [12]).

RESULTS AND DISCUSSION

Figure 3 plots the experimentally determined values of $D^P_{H_2O-Air,eff} = D^P_{H_2O-Air}/\tau$ calculated from Eq. (2), as affected by Kn and d. The indicated uncertainties in $D^P_{H_2O-Air}/\tau$ were calculated from Eq. (2) by comprehensively propagating estimated uncertainty in measuring barrier porosity (determined gravimetrically [12]), barrier thickness [12], $dm_{tot}(t)/dt$, barrier temperature, apparatus temperature, ambient pressure, evaporator geometry, liquid reservoir volume, and sweep gas velocity. Uncertainties in d (and thus Kn) arise from known uncertainty in measuring pore diameter [12].

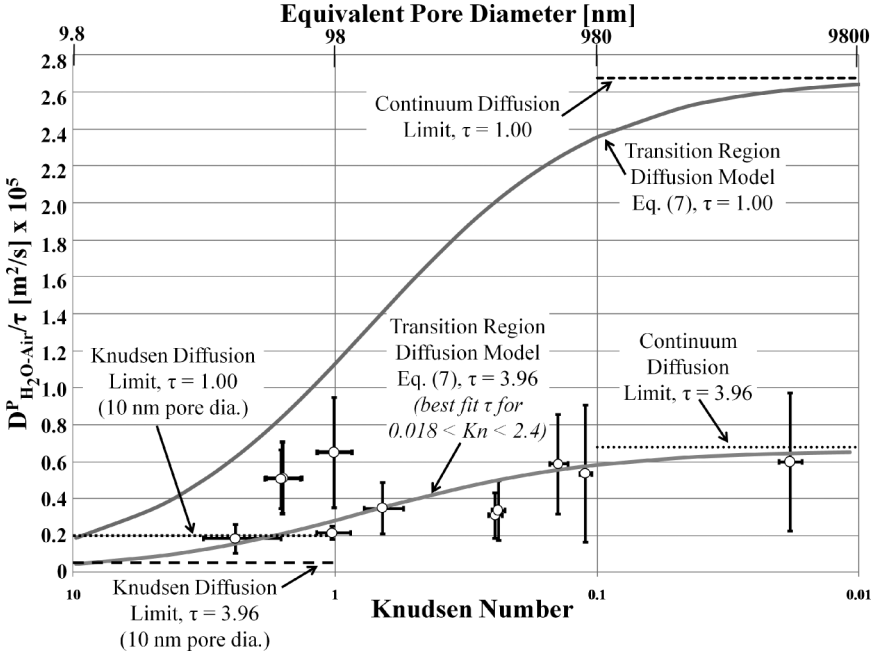

Figure 3 Measured (data points) and predicted (smooth curves) effective diffusivities $D^P_{H_2O-Air}/\tau$ for dilute water vapor in air in nanoscale pores of track-etched polycarbonate barriers as affected by Knudsen number, Kn (or pore diameter, upper abscissa). Kn was varied by changing pore diameter at a constant total pressure of 0.101 MPa. The equivalent pore diameter (upper abscissa) corresponding to the Kn on the lower abscissa was calculated using the mean free path at the average barrier temperature (307 K) and ambient pressure (0.101 MPa).

To compare what was actually measured, that is, $D^P_{H_2O-Air}/\tau$, with model predictions that account for irregularities in pore geometry, we modified Eq. (6) to explicitly include tortuosity (by multiplying each side by τ). We also employed data and dimensional correlations for D_{H_2O-Air} and D_{Kn} from the literature [31]. The resulting modified form of Eq. (6) [12] is

$$\frac{\tau}{D^P_{H_2O-Air}} = \tau \left(\frac{1}{1.87 \times 10^{-10} \left(\frac{T^{2.072}}{P} \right)} + \frac{1}{97\left(\frac{d}{2}\right)\sqrt{\left(\frac{T}{M_{H_2O}}\right)}} \right); \tag{7}$$

$$280\ \text{K} \leq T \leq 450\ \text{K}, 0.01 \leq Kn \leq 10$$

where d is in meters, T is temperature in Kelvins, P is total pressure in atmospheres (1 atm = 0.1013 MPa), M_{H_2O} is the molecular weight of water in g/g-mol, $D^P_{H_2O-Air}$ is in m^2/s, and τ is dimensionless. Figure 3 shows predictions of $D^P_{H_2O-Air}/\tau$ from Eq. (7) for $\tau = 1.00$, a benchmark case where departures from ideal pore geometry do not affect vapor diffusion. The predictions qualitatively capture the broad trend of decreasing $D^P_{H_2O-Air}/\tau$ with declining d evident in the present measurements. However, this version of the model significantly overpredicts the measured $D^P_{H_2O-Air}/\tau$ values for $2.4 > Kn > 0.018$ (39 nm $< d <$ 5,400 nm), implying that tortuosity effects are important for all of the pore sizes of Table 1. To quantify effects of irregular pore geometry we deduced a best fit value of τ by least squares regression of the experimental $D^P_{H_2O-Air}/\tau$ data in Figure 3 against predictions of Eq. (7) using the average pore temperature of 307 K and an average pressure of 0.101 MPa. This analysis assumes that any disagreements between a measured and predicted $D^P_{H_2O-Air}/\tau$ are caused entirely by deviations in pore geometry from isolated through-pores of right circular cylindrical geometry with axes parallel to the direction of diffusion and normal to the barrier face and that the consequences of these imperfections for modeling pore diffusivity are fully represented by a single, pore-size independent tortuosity. To launch the regression we calculated initial values of $D^P_{H_2O-Air}/\tau$ by assuming $\tau = 1.00$ in Eq. (7). The resulting best fit value of τ was 3.96. Figure 3 also presents values of $D^P_{H_2O-Air}/\tau$ at 307 K and 0.101 MPa, predicted from Eq. (7) for the limiting cases of pore transport only by molecular diffusion, that is, D_{H_2O-Air}/τ, or only by Knudsen diffusion, that is, D_{Kn}/τ (for $d = 10$ nm), for $\tau = 1.00$ and $\tau = 3.96$.

Figure 3 implies that $D^P_{H_2O-Air}/\tau$ values predicted from Eq. (7) for $\tau = 3.96$ rather than 1.00 are in substantially better agreement with the data. This is quantitatively supported by the much lower standard error of the estimate for $\tau = 3.96$; that is, 1.89×10^{-6} m^2/s vs. 1.26×10^{-5} m^2/s for $\tau = 1$. If $\tau = 1$ all of the pores would be isolated through-pores of right circular cylindrical geometry running parallel to the direction of diffusion with axes normal to the barrier face. A τ of $\sim$4 indicates that our barrier pore geometry departs significantly from this ideal. SEM images of argon-ion polished edges of a barrier with pores of nominal ID 95 $\pm$ 14 nm (Figure 1) and 406 $\pm$ 19 nm (shown in Traum [12]) confirm deviations in pore geometry from isolated through-pores. Because only the portions of pore tracks within $\sim$100 nm of the cross-sectional surface are visible in Figure 1, short tracks indicate pores highly inclined to a path normal to the barrier face. The angle, Θ, of these tracks to the barrier surface normal can be estimated from $\cos\Theta = L_{vis}/L$ where L_{vis} is the *visible* pore track in Figure 1. The smaller values of L_{vis} in Figure 1 imply that the

maximum Θ may exceed 80°. If the distribution of Θs for each barrier, which is dictated by details of the track etching manufacturing process, were known, a distribution of lengths L_{in} for the inclined pores could be estimated from $L_{in} = L/\cos\Theta$. A further imperfection in pore geometry, also indicated in Figure 1, arises if two or more pore channels intersect. This can create complex three-dimensional networks that may further lengthen the diffusion pathway by allowing water vapor to backtrack before it exits the barrier. In summary, inspection of Figure 1 implies that use of the barrier thickness L in Eq. (2) underestimates the diffusion path, necessitating a correction of $D^P_{H_2O-Air}$ by a $\tau > 1$. Moreover, the resulting best-fitted τ of 4 is consistent with Satterfield [32] and Satterfield and Cadle [33], who found τ from 2.8 to 7.3 for diffusion in 11 pelleted commercial porous catalysts. They used a parallel path model, based on methods of Johnson and Stewart [34], to account for the known pore size distributions of the catalysts. For 10 of the catalysts studied, the flux was in the Knudsen and transition regime; catalyst porosities and specific surface areas ranged from 0.35 to 0.53 and 6.4 to 302 m^2/g, respectively [32, 33].

CONCLUSIONS

When barrier pore diameter d decreases from 5,400 to 39 nm, resulting in an increase in Kn at a constant pressure of 0.101 MPa from 0.018 to 2.4, measured effective pore diffusivities for dilute water vapor in 0.101 MPa air, $D^P_{H_2O-Air}/\tau$, decrease in accord with a model Eq. (7), which equates total pore diffusion resistance to the sum of the molecular (bulk; $Kn \leq 0.01$) and Knudsen ($Kn \geq 10$) diffusion resistances *and* corrects for irregular pore geometry via a single tortuosity, τ, which is assumed to remain the same for all pore sizes. In general τ may vary with pore size. Using a $\tau = 3.96$ best fitted to the present data, the predicted $D^P_{H_2O-Air}/\tau$s are in good quantitative agreement with the $D^P_{H_2O-Air}/\tau$s measured for d from 5,400 to 39 nm.

REFERENCES

1. G. Chen, *Nanoscale Energy Transport and Conversion: A Parallel Treatment of Electrons, Molecules, Phonons, and Photons*, Oxford University Press, New York, 2005.
2. D.W. Johnson, C. Yavuzturk, J. Pruis, Analysis of Heat and Mass Transfer Phenomena in Hollow Fiber Membranes Used for Evaporative Cooling, *Journal of Membrane Science*, Vol. 227, pp. 159–171, 2003.
3. T. Pietrass, Carbon-Based Membranes, *MRS Bulletin*, Vol. 31, pp. 765–769, 2006.
4. D.S. Sholl and Y.H. Ma, Dense Metal Membranes for the Production of High-Purity Hydrogen, *MRS Bulletin*, Vol. 31, pp. 770–773, 2006.
5. J.D. Perry, K. Nagai, and W.J. Koros, Polymer Membranes for Hydrogen Separations, *MRS Bulletin*, Vol. 31, pp. 745–749, 2006.
6. C. Matranga, B. Bockrath, N. Chopra, B. Hinds, R. Andrews, Raman Spectroscopic Investigation of Gas Interactions with an Aligned Multiwalled Carbon Nanotube Membrane, *Langmuir*, Vol. 22, pp. 1235–1240, 2006.
7. C.N. Satterfield, *Heterogeneous Catalysis in Industrial Practice*, 2nd ed., McGraw-Hill, New York, 1991.
8. J. Kärger and D.M. Ruthven, *Diffusion in Zeolites and Other Microporous Solids*, Wiley, New York, 1992.
9. E.L. Cussler, *Diffusion: Mass Transfer in Fluid Systems*, 2nd ed., Cambridge University Press, New York, 1997.
10. M.E. Findley, V.V. Tanna, Y.B. Rao, and C.L. Yeh, Mass and Heat Transfer Relations in Evaporation through Porous Membranes, *AIChE Journal*, Vol. 15, pp. 483–489, 1969.

11. P. Gibson, H. Schreuder-Gibson, and D. Rivin, Transport Properties of Porous Membranes Based on Electrospun Nanofibers, *Colloids and Surfaces A*, Vol. 187, pp. 469–481, 2001.
12. M.J. Traum, Latent Heat Fluxes through Nano-Engineered Porous Materials, Doctoral thesis, Massachusetts Institute of Technology, Cambridge, MA, USA, 2007.
13. M.J. Traum, P. Griffith, E.L. Thomas, and W.A. Peters, Latent Heat Fluxes through Soft Materials with Micro-truss Architectures, *ASME Journal of Heat Transfer*, Vol. 130, pp. 042403–1–042403–11, 2008.
14. C. Cercignani, *Rarefied Gas Dynamics: From Basic Concepts to Actual Calculations*, Cambridge University Press, New York, 2000.
15. G.E. Karniadakis and A. Beskök, *Micro Flows: Fundamentals and Simulation*, Springer, New York, 2002.
16. W.G. Pollard and R.D. Present, On Gaseous Self-Diffusion in Long Capillary Tubes, *Physical Review*, Vol. 73, pp. 762–774, 1948.
17. R.D. Present, *Kinetic Theory of Gases*, McGraw-Hill, New York, 1958.
18. R. Defay, I. Prigogine, and A. Bellemans, *Surface Tension and Adsorption*, Longmans, Green & Co., London, 1966.
19. A.W. Adamson and A.P. Gast, *Physical Chemistry of Surfaces*, Wiley, New York, 1997.
20. N.V. Churaev and A.K. Galwey, *Liquid and Vapor Flows in Porous Bodies: Surface Phenomena*, M.N. Churaeva (Trans.) and A. Galwey (Ed.), Gordon and Breach, Amsterdam, 2000.
21. R.C. Tolman, The Effect of Droplet Size on Surface Tension, *Journal of Chemical Physics*, Vol. 17, pp. 333–337, 1949.
22. W.K. Kegel, On the Variation of the Interfacial Tension with Cluster Size in Connection to Homogeneous Nucleation from the Vapor Phase, *Journal of Chemical Physics*, Vol. 102, pp. 1094–1095, 1995.
23. D.S. Sholl, Understanding Macroscopic Diffusion of Adsorbed Molecules in Crystalline Nanoporous Materials via Atomistic Simulations, *Accounts of Chemical Research*, Vol. 39, pp. 403–411, 2006.
24. N. Giovambattista, P.J. Rossky, P.G. Debenedetti, Effect of Pressure on the Phase Behavior and Structure of Water Confined between Nanoscale Hydrophobic and Hydrophilic Plates, *Physical Review E*, Vol. 73, pp. 041604-1–041604-14, 2006.
25. M. Knudsen, *The Kinetic Theory of Gases: Some Modern Aspects*, 3rd ed., John Wiley & Sons, New York, 1952.
26. W. Gaede, Die äuβere Reibung der Gase (The External Friction of Gases), *Annalen der Physik (Annals of Physics)*, Vol. 41, pp. 289–336, 1913.
27. H. Adzumi, Studies on the Flow of Gaseous Mixtures through Capillaries II: The Molecular Flow of Gaseous Mixtures, *Bulletin of the Chemical Society of Japan*, Vol. 12, pp. 285–291, 1937.
28. S.A. Tison, Experimental Data and Theoretical Modeling of Gas Flows through Metal Capillary Leaks, *Vacuum*, Vol. 44, pp. 1171–1175, 1993.
29. S. Gruener and P. Huber, Knudsen Diffusion in Silicon Nanochannels, *Physical Review Letters*, Vol. 100, pp. 064502-1–064502-4, 2008.
30. S. Roy, S.M. Cooper, M. Meyyappan, and B.A. Cruden, Single Component Gas Transport through 10 nm Pores: Experimental Data and Hydrodynamic Prediction, *Journal of Membrane Science*, Vol. 253, pp. 209–215, 2005.
31. A.F. Mills, *Basic Heat and Mass Transfer*, 2nd ed., Prentice Hall, Upper Saddler River, NJ, 1999.
32. C.N. Satterfield, *Heterogeneous Catalysis in Practice*, McGraw-Hill, New York, 1980.
33. C.N. Satterfield and P.J. Cadle, Diffusion in Commercially Manufactured Pelleted Catalysts, *Industrial and Engineering Chemistry Process Design and Development*, Vol. 7, pp. 256–260, 1968.
34. M.F.L. Johnson and W.E. Stewart, Pore Structure and Gaseous Diffusion in Solid Catalysts, *Journal of Catalysis*, Vol. 4, pp. 248–252, 1965.